PANAMGEO CHILE 2024
17th PAN-AMERICAN CONFERENCE ON SOIL MECHANICS AND GEOTECHNICAL ENGINEERING | 2nd LATIN-AMERICAN REGIONAL CONFERENCE OF IAEG
LA SERENA • CHILE / NOVEMBER 12 - 16, 2024

Proceedings of the 17th Pan-American Conference on Soil Mechanics and Geotechnical Engineering (XVII PCSMGE), and 2nd Latin-American Regional Conference of the International Association for Engineering Geology and the Environment (IAEG), La Serena Chile, 2024.

Post-failure modelling of Las Palmas tailings dam with the Material Point Method

Modelación del post-colapso del tranque de relaves Las Palmas usando el Método del Punto Material

Luis Lemus, Bryan Harris, Andrea Bravo & Jaime Rodríguez
Departamento de Ingeniería en Obras Civiles, Universidad de La Serena, Chile, llemus@userena.cl

ABSTRACT: In recent years, post-failure analysis has gained prominence in geotechnical and mining industries for risk assessment and mitigation actions. Estimating runout from tailings dam failures is now a regulatory requirement for designing, operating, and closing tailings storage facilities (TSF's). The key challenge lies in modeling large deformations while considering mechanics of continuum soil behavior. The material point method (MPM), a continuum mechanics approach, offers promise due to its efficiency in modeling large deformations. It proves valuable for studying the entire instability process, including static stability, failure initiation, post-failure behavior, and subsequent runout. This study applies MPM to a real case: the collapse of Las Palmas tailing dam triggered by the Maule earthquake in Chile (8.8 M_w) in 2010. The dam is located approximately 30 km northwest of the city of Talca in the Maule region of Chile. The computational model focuses on a two-dimensional plane strain state with a fully saturated porous media and coupled hydro-mechanical formulation. Results encompass velocities, deformations, displacements, and final deposition patterns. Notably, the calculated runout distance aligns well with post-collapse reconnaissance, validating the method's capacity in replicating real cases. This research advances our understanding of failure mechanisms and contributes to the risk management in mining industry.

KEYWORDS: Tailing dam failure, material point method, large deformation modeling

1 INTRODUCTION

Tailings deposits are essential geotechnical structures in the mining industry. Nowadays, despite having high standards in their design, total or partial collapses still occur, primarily due to the occurrence of extreme natural events, operational management failures, and deficiencies in design. In fact, it has long been recognized that tailings deposits pose a high risk in terms of mechanical instability (Blight 1997). A review of the main causes of failure or collapse of tailings deposits worldwide indicates that they originate from the occurrence of large earthquakes, infiltrations, overflow, and foundation soil instability (ICOLD 2001, Troncoso 2002, Davies 2002, Rico et al. 2008, Azam & Li 2010, Ishihara et al. 2015, Villavicencio et al. 2014). In Chile, the most significant failures mainly occur due to the liquefaction phenomenon (Dobry & Alvarez 1967, Castro & Troncoso 1989, Troncoso et al. 1993, GEER 2010, Verdugo et al. 2012, Kossoff et al. 2014, Verdugo & González 2015, Villavicencio et al. 2014). This is due to various factors such as a highly seismic environment, upstream construction methodologies, and poor operational control. In general, for liquefaction to occur, it is necessary for a large-magnitude and long-duration earthquake to occur simultaneously; the presence of a water table or extensive saturated zones; and undrained behavior of the soil under dynamic or static loads. In this context, high amounts of water in a tailings deposit are a critical and high-risk condition (Van Zyl 2014).

Following the collapse of a tailings deposit, material empties downstream with great destructive power. For this reason, it is necessary to predict a flood zone, velocities, and the position of the flow to generate eventual mitigation measures or delimitation of safety zones. In this context, the concept of "Dam break Analysis" has been incorporated in various countries, which is associated with predicting the distance traveled or inundation area of the tailings after collapse. To quantify and manage this risk, it is necessary to predict the rupture process and flow dynamics. This analysis is subject to the complexity of unifying in a single calculation the transformation of a solid material into a liquid or semi-liquid state, as occurs in the liquefaction phenomenon. For this reason, as a simplification, many computational models consider tailings as a liquid material, which in some cases could behave like a viscous fluid.

In order to provide a practical solution to the analysis of post-collapse of this type of structure or landslides (similar phenomena), several calculation methods have been developed, among which stand out those based on simplified numerical models (Jeyapalan et al. 1981, Jeyapalan et al. 1983, Hungr 1995), and others of empirical formulation taking information from documented historical collapses (Picciullo et al. 2022, Larrauri & Lall 2018, Rico et al. 2008; Lucia et al 1981). In recent decades, progress has been made in understanding post-collapse, developing computational models capable of predicting the kinematics of tailings flow with various methods and applied to various historical cases of rupture (Macedo et al. 2024, Elkhamra et al. 2023, Ghahramani et al. 2022, Lumbroso et al. 2021, Zabala & Alonso 2011).

In Chile, some catastrophic liquefaction flow failures include the collapses of the El Cobre tailings dam in 1965, because of the La Ligua earthquake; and the collapse of the Las Palmas dam during the great Maule earthquake in 2010. This latter case has been studied by various authors (Hernández 2021, Quilodrán 2021, Moss et al. 2019, Gebarth 2016, Bray et al. 2010), demonstrating numerically and experimentally that the seismic-induced liquefaction flow failure was the mechanism that would explain the collapse. In this line, this work is presented as a contribution to understanding the process following the rupture, considering a flow failure, and through computational modeling, proposes the use of the material point method (MPM) for the description as a large deformations problem.

2 THE MATERIAL POINT METHOD

Numerous computational techniques have been developed for addressing large deformation issues in geotechnical engineering, with particular emphasis on simulating the failure initiation, its progression, and the subsequent run-out. Among these methods, the MPM stands out as a promising approach, exhibiting successful applications in various hydro-mechanical coupled scenarios (Zabala & Alonso 2010, Yerro et al. 2015, Bandara & Soga 2015; Ceccato & Simonini 2016, Bandara et al. 2016, Ceccato et al. 2019b, Pinyol et al. 2017, Wang et al. 2018, Lei et al. 2020). Originating from Sulsky et al. (1994, 1995), MPM is regarded as a hybrid method, combining aspects of mesh-free techniques with traditional finite element methods (FEM).

In MPM, the continuum is discretized into a collection of material points, each representing a subdomain and encompassing all pertinent parameters, scalars, and vector fields. Additionally, a fixed background computational mesh is employed during calculations to solve the momentum equations across the entire problem domain and over successive time steps. Utilizing standard interpolation functions from FEM, information is transferred, and properties are updated between grid nodes and their corresponding material points at each incremental time step. This Eulerian-Lagrangian representation of the domain offers the advantage of obviating the need for mesh generation and regeneration, a common requirement in classical FEM approaches. To review additional details about the algorithm of calculation, it is recommended consulting Alonso et al. (2019) and Soga et al. (2016) for geotechnical engineering applications. In this work, the governing equations used correspond to those formulated to describe a fully saturated media, which are presented below.

A saturated fully coupled formulation in MPM is performed here and the 2-phase-1-point MPM approach to the dynamic behaviour of saturated porous media has been considered in terms of the generalised Biot's formulation (Zienkiewicz & Shiomi 1984). The $v_s - v_l$ formulation (solid and liquid velocities) for saturated media in MPM was stablished by (Jassim et al. 2013). The governing momentum balance equation of the liquid phase (per unit volume of liquid) can be written as follows,

$$\rho_l a_l = \nabla p_l - \frac{n\mu_l}{k_l}\left(v_l - v_s\right) + \rho_l b \qquad (1)$$

where a_l is the acceleration of the liquid phase, v_l and v_s are the total velocities of the liquid and solid phases, respectively, b is the body force vector, ρ_l is the liquid pressure, ρ_l is the density of the liquid phase, μ_L is the dynamic viscosity of the liquid, k_l is the intrinsic permeability of the liquid, and n is the porosity. This equation illustrates the so-called generalised Darcy's law.

The momentum balance of the mixture (per unit volume of the mixture) can be written as:

$$(1 - n)\rho_s a_s + n\rho_l a_l = \nabla\cdot\sigma + \rho_m b \qquad (2)$$

$$\rho_m = \rho_s(1 - n) + \rho_l n \qquad (3)$$

where a_s is the acceleration of the solid particles, σ is the Cauchy total stress tensor of the mixture, ρ_s is the density of the solid particles, ρ_m is the density of the mixture. The mass of the porous media must be separately conserved for each constituent in all calculations. In the case of the solid phase, the solid particles are considered incompressible ($\partial\rho_s/\partial t \approx 0$), therefore the conservation of mass of the solid phase becomes the following expression, which describes the material derivative of the porosity.

$$\frac{dn}{dt} - (1 - n)\nabla\cdot v_s = 0 \qquad (4)$$

The mass balance of the liquid phase can be written analogously to Eq. (4) as

$$\frac{dp_l}{dt} = \frac{K_f}{n}\left[\nabla\cdot v_l + (1 - n)\nabla\cdot v_s\right] \qquad (5)$$

where K_f is the liquid bulk modulus, equivalent to the reciprocal of the liquid compressibility ($K_f = \frac{-1}{\beta_m}$).

3 POST-FAILURE MODELLING OF LAS PALMAS TAILING DAM

The Las Palmas tailings dam is part of a former abandoned gold mining operation (Villavicencio et al., 2014), located near the city of Talca in the Pencahue city in the Maule Region, Chile (See Figure 1). After the earthquake that occurred in Chile on February 27, 2010, partial collapse of the Las Palmas mine tailings occurred, obstructing the local drainage network, and altering the local morphology due to the tailings flooding (DICTUC, 2010). Due to the seismic event, liquefaction occurred in its material, where this failure took two directions, one towards the East, with an approximate displacement of 165 m from the edge of the reservoir, and another towards the South, with an approximate displacement of 350 m from the edge of the reservoir. The liquefiable flow had an approximate thickness of 1.5 to 4.0 m in some places (Gebhart 2016; Bray et al. 2010).

The interplate earthquake on February 27, 2010, with a magnitude of M_w 8.8 and a depth of 35 km off the coast of the Maule Region, represented the sixth-largest earthquake recorded in the world since 1900.

n

A liquefaction failure was observed at the base level of the retaining dam, apparently due to saturation of the few lower meters (0.5 to 1 m) caused by undetected groundwater. This saturation zone apparently was not detected at the time of the closure of the deposit (Villavicencio et al. 2014).

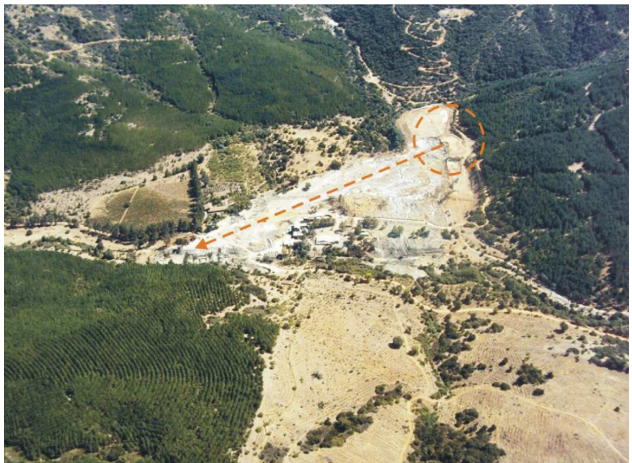

Figure 2. Las Palmas tailing dam after the collapse generated by the 27 February 2010 earthquake (Villavicencio et al. 2014)

3.1 *Geometric and construction stages configuration*

The tailings dam was built on existing terrain with a slope descending towards the South and East. Above, it had a maximum upper slope of 4:1 (horizontal and vertical) and a maximum lower slope of 15:1, horizontal and vertical (Gebhart 2016). In Figure 3 is showed the construction sequence of the dam, which consisted of 4 individual stages developed over a period of 17 years, between 1981 and 1998 (Moss et al. 2019, Gebhart 2016). The sequence began with the construction of stage one, which consisted of a retaining wall and placement of hydraulic fill tailings (finely crushed solid). Following this, as shown in Figure 3, stage two was positioned upstream at the same height as the initial wall. Subsequently, on these two completed stages, and using the downstream method, stage three was constructed. Finally, in stage four, walls and tailings were positioned on the material contained in stage three. For the case of retaining walls or embankments, the sandy and granular fraction of the tailing's material was used to generate greater resistance capacity.

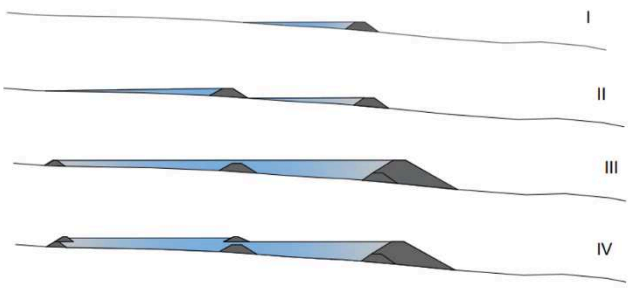

Figure 3. Construction stages of Las Palmas Tailing dam.

To generate the surface of soil foundation, a two-dimensional model is created prior to the failure, along with Google Earth satellite images supplemented with a raster model of the area, to obtain the corresponding contour lines of the terrain using QGIS software as showed in the Figures 4 and 5.

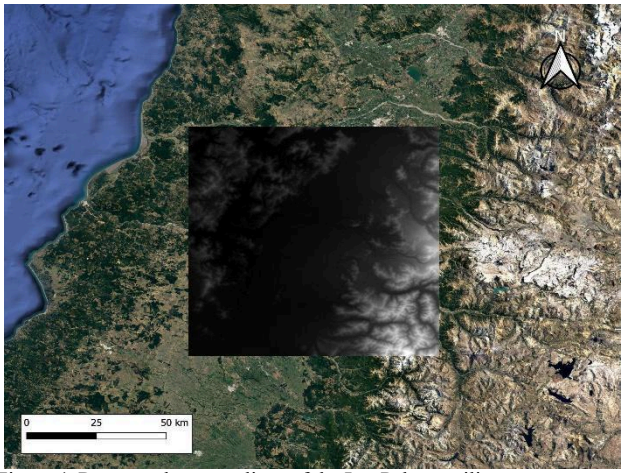

Figure 4. Raster and contour lines of the Las Palmas tailings sector.

With the above information, the slopes where the collapsed material moved were traced, complementing with the geometry of the tailings dam prior to the failure obtained from Hernández (2021). Subsequently, the geometric digital model shown in Figure 7 was developed using AutoCAD Civil 3D software corresponding to the section indicated in Figure 6.

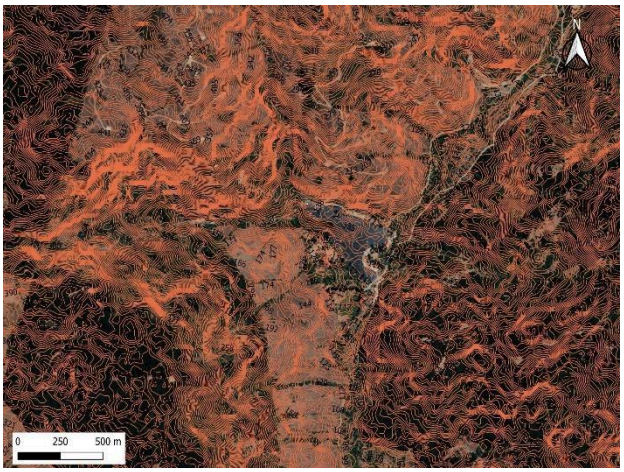

Figure 5. Contour lines generated in QGIS.

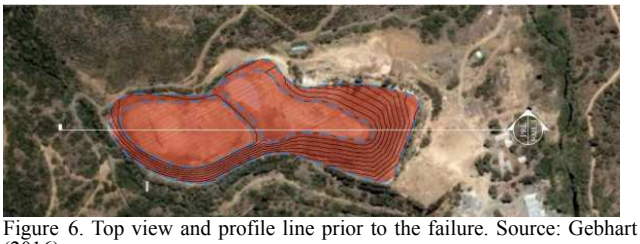

Figure 6. Top view and profile line prior to the failure. Source: Gebhart (2016).

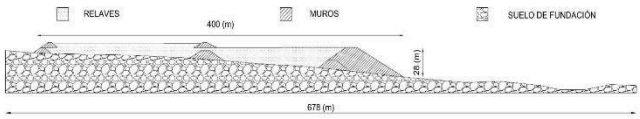

Figure 7. Cross-sectional profile of the two-dimensional geometric model of the Las Palmas tailings dam prior to the failure.

3.2 *Geotechnical characterization and adopted parameters*

According to the drilling records, triaxial tests, geotechnical characterization, and the post-collapse reconnaissance work of the deposit (Bray et al. 2010; Gebhart 2016), it was determined that the computational model considered three types of materials: tailings, walls, and foundation soil. The tailings from the dam are composed of a sandy silt material with a low percentage of silty sand susceptible to liquefaction. The constitutive model used for the tailings corresponds to the classical Mohr Coulomb model for both liquefied and non-liquefied material.

Non-Liquefied Tailings: For modeling the non-liquefied tailings material, a drained condition was considered (cohesion of 0 kPa), where, due to the frictional resistance of the silts, "peak" and residual parameters of this material were obtained. The residual parameters were chosen to determine the internal friction angle corresponding to 21°, as it best represented the mobilized soil resistance within the flow failure. The Young's modulus was calculated considering the number of blows from the drillings obtained from the data provided by Gebhart (2016), resulting in different modulus values from which an average value of 1,341

kPa was calculated to represent the material. As for the Poisson's ratio, a value of 0.325 was adopted from specialized literature considering various soil classifications.

Liquefied Tailings: The liquefied tailings material has a residual post-liquefaction strength of 8.28 kPa obtained from the conclusions of Gebhart (2016). It has a friction angle of 0° due to the deficiency in its load-bearing capacity if the material liquefied entirely due to the seismic event. For the Young's modulus, Poisson's ratio, and other parameters, the same values as the non-liquefied tailings were retained.

Sand walls: The material used to construct the walls or containment dikes is classified as silty sand (SM) with a low percentage of silt. In the models created, it was configured using the classical Mohr Coulomb constitutive model.

Non-Liquefied walls: Regarding the parameters of this material, a friction angle of 26° and a cohesion of 38.3 kPa were assigned, obtained from triaxial tests under consolidated undrained conditions. The Young's modulus of 5,724 kPa, similar to the tailings, was obtained from the number of blows of the SPT test conducted in situ. A Poisson's ratio of 0.3 was defined based on existing tables in specialized literature associated with various soil classifications.

Liquefied sand walls: the parameters of Young's modulus (E) and Poisson's ratio (ν) remain unchanged. As for cohesion, a low value is assigned because it is assumed that the collapsed material had no resistance due to the seismic event, with a value of 3 kPa.

Soil foundation: for the analyzed case study was considered as a competent material with high strength that had minimal relevance in the collapse of the deposit. Regardless of this assessment, the material was configured with a linear elastic model with a very high modulus of elasticity to represent it as an impenetrable material. Based on the review of background information, it was confirmed that no failure occurred in the foundation soil, validating the assumption that this material has high strength.

According to this, a resumen of adopted parameters is shown in the following table.

Table 2. Summary of parameters adopted for the model in MPM.

Parameter	Non-Liquefied sand walls	Liquefied sand walls	Non-Liquefied tailings	Liquefied tailings	Soil foundation
n	0.65	0.65	0.65	0.65	0.25
ρ_s (kg/m^3)	2,730	2,730	2,730	2,730	2,700
ρ_l (kg/m^3)	1,000	1,000	1,000	1,000	1,000
k_L(m^2)	$1,0\,x\,10^{-8}$	$1,0\,x\,10^{-8}$	$1,0\,x\,10^{-8}$	$1,0\,x\,10^{-8}$	$1,0\,x\,10^{-5}$
K_f(kPa)	$2,2\,x\,10^{-4}$	$2,2\,x\,10^{-4}$	$2,2\,x\,10^{-4}$	$2,2\,x\,10^{-4}$	$2,2\,x\,10^{-4}$
μ (kPa•s)	1.0 x 10^6	1.0 x 10^6	1.0 x 10^6	1.0 x 10^6	1.0 x 10^6
ν	0.3	0.3	0.325	0.325	0.2
E (kPa)	5,724	5,724	1,341	1,341	200,000
c (kPa)	38.3	5	0	8.28	-
φ (°)	26	3	21	0	-
ψ (°)	0	0	0	0	-

ρ_s: Solid Density; n: Porosity; k_L: Intrinsic permeability; K_f: Bulk modulus of water; μ: Dynamic viscosity; E: Young modulus; ν: Poisson's coefficient; c: Cohesion; φ: Friction angle.

3.3 *Model configurations and computational meshing*

Two calculation phases are considered: a static phase is performed by the application of the gravity loading and a dynamic phase correspond to the collapse. In the Anura3D code, calculation data were established to evaluate the number of time steps (iterations) to be calculated. Each calculation step represents a fraction of time, which in our case was determined to be equivalent to 0.1 seconds per step. Considering a total of 600 time-steps, therefore the real simulation time is 60 s.

The two-dimensional model mesh encompasses the entire computational domain, even where there is initially no material (blue mesh), as depicted in Figure 8. The objective is to fully cover the spatial domain where it is assumed that material will exist when the soil mass moves. In all models created, the mesh consists of triangular linear elements, as shown in Figure 8. For the analyzed deposit, the dimension of the foundation soil elements was set to 5.0 m as it is not relevant in the modeling (unnecessary and time-consuming calculations), while for the tailings, walls, and areas where material could mobilize, it was set to 1.5 m. Additionally, an unstructured mesh of 1.0 m was applied to the interface line between the collapsed tailings and the foundation soil, achieving mesh refinement in the areas of interest (where the material will mobilize) to attain a refined calculation network and avoid interference from overly coarse mesh in the flow of collapsed material. This model consists of 13,674 nodes and 26,690 triangular elements, each of which is composed of three material points equivalent to a total of 80,070 particles.

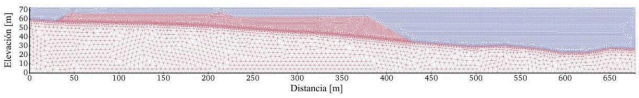

Figure 8. Computational mesh of the model.

The MPM is implemented in Anura3D opensource code (Anura Research Community 2022) in Fortran language. To the simulations in a virtual machine with high calculation performance. The characteristic of the CPU used is detailed in Table 3.

Table 3. CPU characteristics of virtual machine used.

CPU details	
Operating System	Windows 10 Pro, version 22H2, 64 bits, processor x64
Processor	Intel® Xeon® Gold 52218 CPU @ 2.30GHz 2.29 GHz
N° cores	12 Cores de CPU

Storage	500 Gb
Memory (RAM)	64 Gb

3 RESULTS

A static calculation phase is presented, corresponding to the initialization of stress state by quasi-static gravitational loads, defined in two calculation steps. The result at the end of this phase is shown in Figure 9.

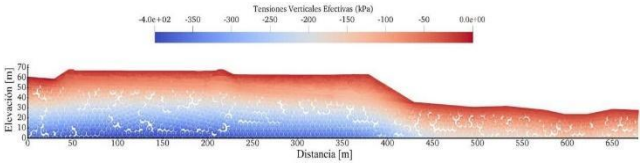

Figure 9. Vertical geostatic stress to initial conditions setup.

The dynamic stage of the model corresponds to the displacement of the materials composing the tailings dam, where one of the objectives of this study is the analysis of the post-collapse scenario. A total of 600 calculation steps, corresponding to 60 s after the static phase, were considered, as this is an appropriate time range for complete collapse to occur and for the dangerous distance to be obtained.

Here the liquefied parameters were used for both the tailings and the downstream walls of the dam. Given the magnitude of a seismic event, it is assumed that the tailings, being very fine and barely compacted materials, liquefy entirely. In the case of the walls, liquefaction was considered as there are records confirming their collapse. Regarding the central walls and those located upstream, they remained in non-liquefied conditions as observed in situ, maintaining their initial position, thus preserving the quasi-static parameters. Figure 10 illustrates the material conditions at the start of the dynamic phase of the model.

Figure 10. Material configuration of the model.

During the dynamic phase, of the initial 60 s of time considered, it only took 49 s for the material to come to a stop, allowing the run-out distance to be visualized. Within this time interval, the material traveled 160 m from the toe of the downstream wall slope (see Figures 11 and 12).

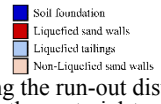

Figure 11. Evolution of position of tailing dam flow failure.

Figure 12. Final deposition of collapsed tailings and initial geometric setup.

According to the information gathered, the collapsed material reached an approximate distance of 165 m. When comparing this result with the computational model, there is agreement in terms of run out distance reached. The difference could be attributed to the fact that, since the focus of the dam modeling was on post-collapse behavior, seismic analysis was not considered. It was assumed that both the tailings and the downstream walls liquefied. Additionally, due to the lack of exact knowledge of some material parameters, common values for a certain soil classification had to be used, and assumptions were made for values for which there were no data.

Additionally, it is observed that during the collapse, the downstream walls (coarse material), as depicted in Figure 13, began to open a path along the slope of land surface. However, during the movement, particles were left behind along the path, causing the tailings (fine material) to spread over the liquefied material of the walls but not to surpass it. Additionally, it is evident that the tailings upstream did not flow due to the non-liquefied parameters of the central walls. Nevertheless, it is observed that the wall in stage IV (central), despite its properties, exhibited deformations in its structure.

Figure 13. Final disposal of constituent materials after the collapse.

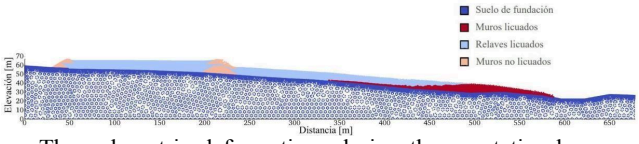

The volumetric deformations during the geostatic phase are shown in Figure 14a small deformation values can be observed, as the materials in this condition still possess a level of non-liquefied material resistance. However, already in the early moments of the dynamic phase, cutting bands are evidenced at

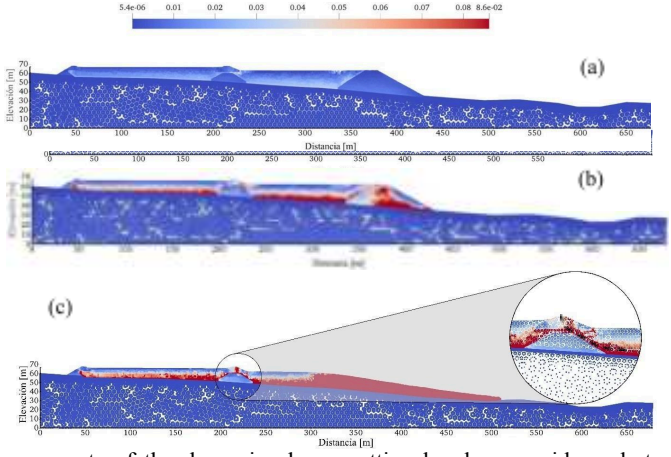

the interfaces and into the principal sand wall (see Figure 14b). Following this, the deformation began to progress backwards, where the shear bands gradually increased due to the liquefied tailings until it completely lost its resistance, causing it to descend as a whole or in block form. At the same time, it is observed how the bands ascended along the slope of the lower central wall until reaching the point of generating deformations and subsequent rupture of the upper wall, as shown in Figure 14c, that agree with real case (see Figure 15).

Figure 14. Volumetric deformation and shear band at the failure initiation.

Figure 15. State of the central walls post-collapse. Source: Gebhart, 2016; Bray et al, 2010. a) Aerial view of the walls and the material and b) Edge of mobilized flow failure.

The description of the tailings flow kinematics is conducted through the tracking of control points located in different areas of the deposit. These points are indicated in Figure 15, where it can be observed that there are differences in the velocities reached, both in terms of magnitude and timing of occurrence. Maximum velocities can be observed at different time instants. Regarding the advance front of the tailings, an average of maximum values is 14 m/s (~50 km/h) reached at about 7 s, highlighting the destructive power of tailing flow that was developed (see Figure 16).

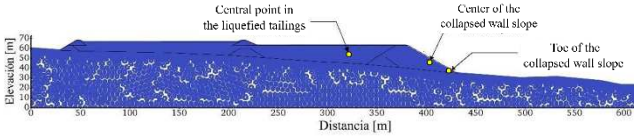

Figure 16. Velocities at different points versus calculation time, a) Central point in liquefied tailings, b) Center of the collapse sand wall, and c) Toe of the collapsed sand wall.

Finally, the displacements of three control points are (a) which are indicated in Figure x, along with their respective evolution over time. The maximum displacement reached is around 180 m in the “Point 3” located at the slope of the dam (See figure 17 and 18). Regarding the displacement of "Point 1" (tailings material), it is inferred that at approximately 7 seconds, the material begins to slide, where it is observed that at 33 s, a maximum displacement of 70.2 m is generated. After this, the particles begin to stabilize.

As for "Point 2" and "Point 3," corresponding to the collapsed wall, a significant difference can be appreciated between their values due to their positions. "Point 3" shows a pronounced curve because in the first 10 s, the material moved approximately 100 m, reaching the maximum collapse displacement (179.8 m) at 49 s. The reason for this is that being on the downstream slope of the collapsed wall leads to greater movement from the beginning of the failure without resistance from a material holding it back. On the other hand, "Point 2" only traveled a distance of 2.88, starting its movement at approximately 13 s and stopping at 35 s. This is because it is located at the back of the base of the wall, causing the tailings material to pass over this point, reducing its displacement.

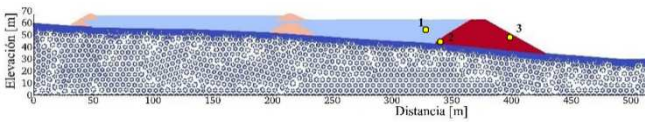

Figure 17. Points selected for displacements analysis.

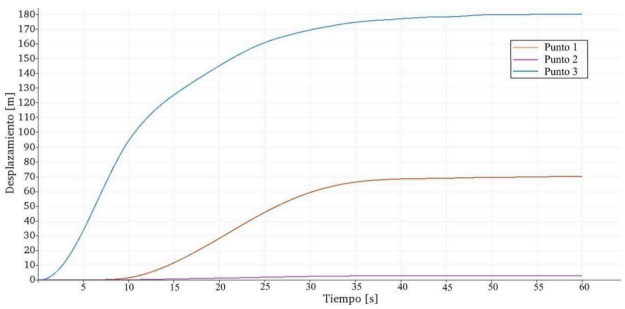

Figure 18. Displacements over the time for three points.

4 CONCLUSIONS

This study adds value to MPM to understanding the behavior of tailings deposits after failure, due to its unique capabilities that allow for modeling problems of large soil deformation. The results obtained in terms of travel distance are validated according to the information collected on-site after the collapse of the deposit. In this regard, approximately 160 m measured from the toe of the sand wall slope has been estimated, a value that fits well with what was observed, however in other point a maximus displacement calculated is about 180 m. Regarding the evolution of the failure in terms of deformations and cutting bands, the morphology of the collapse influenced by assuming liquefied material parameters in the dynamic phase could be replicated. In addition, the estimation of velocities achieved in the model stands out, which could validate the destructive potential of the tailings flow. Nevertheless, there is still room for improvement in terms of describing the failure process, which could be achieved by integrating advanced constitutive models that include the liquefaction phenomenon considering seismic loading.

It would be interesting for future studies to make additional improvements to the presented model. This could include integrating a more advanced constitutive model to provide the software with more precise information about the behavior of tailings and liquefaction-induced seismic failure. Furthermore, with proper computational implementation, a finer mesh could be generated to avoid interference from an overly coarse mesh in the flow of collapsed material. Additionally, more material points could be added to the triangular elements to prevent numerical instabilities. Finally, integrating seismic conditions and dynamic parameters, as well as developing a three-dimensional computational model, would contribute to creating a more reliable model of the event and predicting future collapses.

5 ACKNOWLEDGEMENTS

The authors would like to thank the Department of Civil Engineering at the University of La Serena for their support in this work. Luis Lemus acknowledges the National Agency for Research and Development (ANID) of the Government of Chile for the doctoral scholarship abroad (CONICYT-PCHA/Doctorado Internacional/2017-72180231) and to the financial support of FIULS 2030 through the project "FIULS 2030", code 18ENI2-104235, from the program "New Engineering for 2030 in Regions - Implementation Stage.

6 REFERENCES

Alonso, E., Soga, K., Fern, J., & Rohe, A. (Eds.). (2019). The Material Point Method for Geotechnical Engineering: A Practical Guide. CRC Press, Taylor & Francis Group.

Anura3D MPM Research Community (2022). https://github.com/Anura3D/Anura3D_OpenSource

Azam, S. and Li, Q. (2010). Tailings dam failures: a review of the last one hundred years. Geotechnical News/Waste Geotechnics, pp. 50-53.

Blight, G. (1997). Destructive mudflows as a consequence of tailings dyke failures. Proceedings of the ICE – Geotechnical Engineering, vol 125 (1), pp. 9–18.

Bray, J., & et. al. (2010). Geo-engineering Reconnaissance of the 2010 Maule, Chile Earthquake. Geo-engineering extreme events reconnaissance (GEER) association, Report No. GEER-022.

Castro, G. and Troncoso, J. (1989). Effects of 1985 Chilean earthquake on three tailing dams. In Proceedings of the Fifth Chilean Conference on Seismology and Earthquake Engineering, Santiago, Chile.

Concha Larrauri, P., & Lall, U. (2018). Tailings dams failures: Updated statistical model for discharge volume and runout. Environments, 5(2), 28.

Davies, M. (2002) 'Tailings impoundment failures: Are geotechnical engineers listening?', Waste Geotechnics, Geotechnical News, pp. 31–36.

DICTUC. (2010). Evaluación preliminar de contingencia en tranque de relaves Las Palmas, Sector Pencahue, Región del Maule. Repositorio.uc.chromeextension://efaidnbmnnnibpcajpcglclefindmkaj/https://bibliotecadigital.ciren.cl/bitstream/handle/20.500.13082/32496/DGA_2010_evaluacion_tranque_Las_Palmas_Pencahue_Region_Maule.pdf?sequence=1

Dobry, R., and Alvarez, L. (1967). Seismic failures of Chilean tailings dams. Journal of the Soil Mechanics and Foundations Division, ASCE, 93(6): 237–260.

Elkhamra, Y., Chen, H., & Stark, T. (2023). Inverse analysis of Cadia tailings dam failure. Geo-Congress 2023.

GEER Geo-Engineering Extreme Events Reconnaissance Association (2010). Dams, levees, and mine tailings dams. In Turning disaster into knowledge: geo-engineering reconnaissance of the 2010 Maule, Chile Earthquake. Edited by J. Bray and D. Frost. pp. 204–226.

Gebhart, T. R. (2016). Post-Liquefaction Residual Strength Assessment of the Las Palmas, Chile Tailings Failure. chrome-extension://efaidnbmnnnibpcajpcglclefindmkaj/https://digitalcommons.calpoly.edu/cgi/viewcontent.cgi?article=2848&context=theses

Ghahramani, N., Chen, H. J., Clohan, D., Liu, S., Llano-Serna, M., Rana, N. M., McDougall, S., Evans, S. G., & Take, W. A. (2022). A benchmarking study of four numerical runout models for the simulation of tailings flows. The Science of the Total Environment, 827(154245), 154245.

Hernández A. (2021). Colapso del tranque de relaves Las Palmas durante el sismo del Maule 2010. https://doi.org/10.7764/tesisUC/ING/57461

ICOLD (2001). Tailings dams - risk of dangerous occurrences, lessons learnt from practical experiences. Bulletin 121. United Nations Environmental Programme (UNEP), Division of Technology, Industry and Economics (DTIE) and International Commission on Large Dams (ICOLD), Paris.

Hungr, O. (1995). A model for the runout analysis of rapid flow slides, debris flows, and avalanches, Can. Geotech. J, vol. 32, pp. 610–623.

Ishihara K., Ueno K., Yamada S., Yasuda S. and Yoneoka T (2015). Breach of a tailings dam in the 2011 earthquake in Japan. Soil Dynamics and Earthquake Engineering, 68 (2015) 3–22

Jassim, I., Stolle, D., Vermeer, P., (2013). Two-phase dynamic analysis by material point method. International Journal for Numerical and Analytical Methods in Geomechanics numerical and Analytical Methods in Geomechanics 37, 2502–2522.

Jeyapalan, J., Duncan, M., Seed H., (1981). Summary of research on analyses of flow failures of mine tailings impoundment. Information Circular 8857, Technology Transfer Workshop on Mine Waste Disposal Techniques, U.S Bureau of Mines, Denver, CO., pp. 54–61.

Jeyapalan, J., Duncan, M., Seed H., (1983). Analyses of flow failures of mine tailings dams, J. Geotech, Engrg, vol 109, pp. 150–171.

Kossoff D., Dubbin W.E., Alfredsson M., Edwards S.J., Macklin M.G., Hudson-Edwards K.A. (2014). Mine Tailings Dams: Characteristics, Failure, Environmental Impacts, and Remediation. Applied Geochemistry, Volume 51, December 2014, Pages 229–245

Piciullo, L., Storrøsten, E. B., Liu, Z., Nadim, F., & Lacasse, S. (2022). A new look at the statistics of tailings dam failures. Engineering Geology, 303(106657).

Pinyol, N.M., Alvarado, M., Alonso, E.E. and Zabala, F., (2017). Thermal effects in landslide mobility. Géotechnique 68, 1–18.

Quilodrán C. (2021). Distancia peligrosa tranque de relaves Las Palmas. https://masterieg.uc.cl/wpcontent/uploads/2022/08/A_G_2021_Carlos_Quilodran.pdf

Lucia, P., Duncan, J., and Seed, H. (1981) 'Summary of research on case histories of flow failures of mine tailings impoundments', Technology Transfer Workshop on Mine Waste Disposal Techniques, U.S Bureau of Mines, Denver, CO., pp. 46-53.

Lumbroso, D., Davison, M., Body, R., and Petkovšek, G. (2021). Modelling the Brumadinho tailings dam failure, the subsequent loss of life and how it could have been reduced, Nat. Hazards Earth Syst. Sci., 21, 21–37.

Macedo, J., Yerro, A., Cornejo, R., & Pierce, I. (2024). Cadia TSF failure assessment considering triggering and posttriggering mechanisms. Journal of Geotechnical and Geoenvironmental Engineering, 150(4).

Moss R. E. S., Gebhart T. R., Frost J. D. & Ledezma C. (2019). Flow-failure case history of the Las Palmas, Chile, tailings dam, PEER report 2019/01. (s/f). Berkeley.edu.

Rico M., Benito G., Salgueiro A.R., Díaz-Herrero A. and Pereira H.G. (2008). Reported tailings dam failures a review of the European incidents in the worldwide context. Journal of Hazardous Materials 152 (2008) 846–852.

Rico M., Benito G. and Díaz-Herrero A. (2008) Floods from Tailings dam failures. Journal of Hazardous Materials 154 (2008) 79–87.

Soga, K., Alonso, E., Yerro, A., Kumar, K., Bandara, S., (2016). Trends in large-deformation analysis of landslide mass movements with particular emphasis on the material point method. Géotechnique 66, 248–273.

Sulsky, D., Chen, Z., Schreyer, H., (1994). A particle method for history-dependent materials. Comput. Methods Appl. Mech. Eng. 118, 179–196.

Sulsky, D., Zhou, S.-J., Schreyer, H.L., (1995). Application of a particle-in-cell method to solid mechanics. Comput. Phys. Commun. 87, 236–252.

Van Zyl D. (2014). Plenary Presentation: Holistic approach to mine waste management. 2nd International Seminar on Tailings Management, Gecamin: Tailings 2014, Antofagasta, Chile.

Verdugo R. et al (2012). Seismic Performance of Earth Structures during the February 2010 Maule, Chile, Earthquake: Dams, Levees, Tailings Dams, and Retaining Walls. Earthquake Spectra, Volume 28, No. S1, p.p. S75–S96.

Verdugo R. and González J. (2015). Liquefaction-induced ground damages during the 2010 Chile earthquake. Soil Dynamics and Earthquake Engineering. Volume 79, Part B, p.p. 280–295.

Villavicencio G., Espinace R., Palma J., Fourie A. and Valenzuela P. (2014). Failures of sand tailings dams in a highly seismic country. Can. Geotech. J, vol. 51, pp. 449–464.

Zabala, F. & Alonso, E. E. (2011). Progressive failure of Aznalcóllar dam using the material point method. Géotechnique 61, No. 9, 795–808.

Zienkiewicz, O. C. & Shiomi, T. (1984). Dynamic behaviour of saturated porous media: the generalized Biot formulation and its numerical solution. Int. J. Numer. Analyt. Methods Geomech. 8, No. 1, 71–96.